Sains Malaysiana 55(5)(2026): 825-837
http://doi.org/10.17576/jsm-2026-5505-05

Upcycling Pineapple Stem Waste into PLA-Based Bioplastics: The Role of Maleinized Linseed Oil in Film Performance and Biodegradability

(Mengitar semula Sisa Batang Nanas menjadi Bioplastik Berasaskan PLA: Peranan Minyak Biji Rami Malein dalam Prestasi Filem dan Kebolehuraian Bio)

HATAITHIP SANPROMMA[1], SUPATRA PRATUMSHAT[1,2,*] & TAWEECHAI AMORNSAKCHAI[3]

[1]*Department of Chemistry, Faculty of Science, Naresuan University, Phitsanulok 65000, Thailand*
[2]*Center of Excellence in Biomaterials, Faculty of Science, Naresuan University, Phitsanulok 65000, Thailand*
[3]*Center of Sustainble Energy and Green Materials, Faculty of Science, Mahidol University, Salaya, Phuttamonthon District, Nakhon Pathom 73170, Thailand*

Received: 5 July 2025/Accepted: 6 May 2026

ABSTRACT

This study reports the development of sustainable packaging films based on polylactic acid (PLA) and thermoplastic starch (TPS), utilizing starch extracted from pineapple stem waste, an abundant and underutilized agricultural by-product in Thailand. Maleinized linseed oil (MLO), a fully bio-based compatibilizer, was incorporated to improve interfacial adhesion and enhance mechanical performance. PLA/TPS blends with varying MLO content were processed via twin-screw extrusion and film blowing. Mechanical testing showed that MLO significantly increased elongation at break to 43.21%, and thermal analysis indicated a reduction in T_g, confirming the plasticizing effect of MLO and consistent with an increased interaction index of PLA/15TPS/MLO (5.28) compared to PLA/20TPS (5.03). SEM showed improved phase dispersion. The PLA/10TPS/10MLO blend demonstrates the most balanced properties. Biodegradation tests in soil and simulated marine conditions showed enhanced degradation in TPS-containing blends, although MLO slightly reduced the degradation rate by limiting water diffusion. The integration of agricultural waste valorization and green additives offers a promising route to fabricate biodegradable films suitable for single-use packaging applications, thereby contributing to circular economic efforts.

Keywords: Compatibilizer; maleinized linseed oil (MLO); pineapple stem starch; polylactic acid (PLA); thermoplastic starch (TPS)

ABSTRAK

Kajian ini melaporkan pembangunan filem pembungkusan lestari berasaskan asid polilaktik (PLA) dan kanji termoplastik (TPS) menggunakan kanji yang diekstrak daripada sisa batang nanas, hasil sampingan pertanian yang banyak dan kurang digunakan di Thailand. Minyak biji rami termanjan (MLO), penyerasi berasaskan bio sepenuhnya telah digabungkan untuk meningkatkan lekatan antara muka dan meningkatkan prestasi mekanikal. Campuran PLA/TPS dengan pelbagai kandungan MLO telah diproses melalui penyemperitan skru berkembar dan peniupan filem. Ujian mekanikal menunjukkan bahawa MLO meningkatkan pemanjangan pada takat putus dengan ketara kepada 43.21% dan analisis haba menunjukkan pengurangan T_g, mengesahkan kesan pemplastikan MLO dan tekal dengan peningkatan indeks interaksi PLA/15TPS/MLO (5.28) berbanding PLA/20TPS (5.03). SEM menunjukkan penyebaran fasa yang lebih baik. Campuran PLA/10TPS/10MLO menunjukkan sifat yang paling seimbang. Ujian biodegradasi dalam tanah dan keadaan simulasi marin menunjukkan peningkatan degradasi dalam campuran yang mengandungi TPS, walaupun MLO mengurangkan sedikit kadar degradasi dengan mengehadkan resapan air. Integrasi pengayaan sisa pertanian dan bahan tambahan hijau menawarkan laluan yang berpotensi untuk menghasilkan filem terbiodegradasi yang sesuai untuk aplikasi pembungkusan sekali-guna, sekali gus menyumbang kepada usaha ekonomi kitaran.

Kata kunci: Asid polilaktik (PLA); kanji batang nanas; kanji termoplastik (TPS); minyak biji rami termanjan (MLO); pengserasi

INTRODUCTION

The global plastic pollution crisis is escalating, with an estimated 400 million metric tons of plastic waste generated in 2024. Most plastic packaging is single-use and poorly recycled, leading to long-term environmental contamination. By 2050, plastic in the oceans could outweigh marine life (Atiwesh et al. 2021; Mallick et al. 2020). The discovery of microplastics in human tissues raises alarming health concerns (Logam et al. 2015; Nihart et al. 2025).

To address this, bio-based and biodegradable polymers are being developed. Polylactic acid (PLA), derived from renewable sources, offers high strength and biodegradability but is brittle and degrades slowly. Thermoplastic starch (TPS), a highly biodegradable and economically attractive material from pineapple stem starch (PSS), is an underutilized agricultural waste. Thailand, a major pineapple producer, generates approximately 1.65 million tons of fruit and 2.7 million tons of post-harvest waste annually (Japheth & John 2018). After fruit harvesting, the estimated waste from pineapple cultivation across the country is about 2.7 million tons per year. Instead of burning agricultural waste, converting it to valuable starch could reduce pollution. TPS, especially from pineapple stem waste has high-purity starch content and is rich in amylose. High-amylose starch is ideal for biodegradable plastics; its linear molecular structure enables strong hydrogen bonding (Seung 2020), providing superior mechanical strength, stiffness, higher failure stress, and better film-forming capabilities than those dominated by branched amylopectin from other starches (Aboubakar et al. 2008; Chu et al. 2021; Li et al. 2025; Nakthong, Wongsagonsup & Amornsakchai 2017). However, the properties of TPS are not yet enough for single-use plastic packaging.

Combining PLA and TPS could balance their strengths, but their incompatibility causes phase separation and poor mechanical integrity (Park et al. 2000; Wang et al. 2008). Compatibilizers such as PEG (Ferrarezi et al. 2013), PCL (Sarazin et al. 2008), and isocyanate (Akrami et al. 2016) have been studied but may pose issues such as migration or toxicity (Shlosman et al. 2014). Maleinized linseed oil (MLO) emerges as a promising bio-based alternative, capable of acting as both a biobased plasticizer and a reactive compatibilizer, thereby improving PLA/TPS compatibility through its reactive anhydride groups. This dual mechanism transforms a brittle, immiscible blend into a tougher, more impact-resistant material compared to uncompatibilized systems. Additionally, MLO provides high thermal stability, enhanced degradation resistance, and a 10 °C reduction in the glass transition temperature, offering a sustainable, non-toxic, and cost-effective solution for high-performance biopolymer production (Ferri et al. 2016; Hongsriphan et al. 2020; Liminana et al. 2019). This study investigates the effects of TPS from pineapple stem starch and MLO from the blown film process. The novelty of this work lies not in a single component but in the integration of a non-conventional TPS source, bio-based reactive compatibilization, and morphology control during blown film processing, resulting in a balanced enhancement of mechanical properties and biodegradability.

MATERIALS AND METHODS

MATERIALS

PLA (4043D) was obtained from NatureWorks, with a density of 1.24 g/cm³ and a melt flow index of 6 g/10 min. Dry pineapple stem powder was obtained from TCP HERB, Thailand. Glycerol was supplied by KemAus. Linseed oil (food-grade) was purchased from MySkinRecipes in Thailand. Maleic anhydride (MA) was obtained from Sigma-Aldrich.

THERMOPLASTIC STARCH PREPARATION

Pineapple stem starch was prepared from dried pineapple stems. The stems were ground and then sieved through a 140-mesh screen, after which the fibrous material was removed by filtration. Water was added to the starch to eliminate water-soluble impurities, and the mixture was allowed to settle until phase separation occurred. This washing process was repeated several times until the liquid fraction became clear. Finally, the solid fraction was dried in an oven at 60 °C overnight.

Thermoplastic starch (TPS) was prepared from pineapple stem starch, glycerol, and distilled water at a ratio of 65:30:5 wt%. Initially, the components were manually pre-mixed. Subsequently, the mixture was processed by extrusion using a co-rotating twin-screw extruder (LABTECH Model LTE16-40) with a screw diameter of 16 mm and an L/D ratio of 40. The temperature profile from the feed zone to the metering zone was set at 110, 120, 120, 120, 130, and 130 °C, while the screw speed was maintained at 100 rpm. After extrusion, the material was cooled by air and then cut into pellets.

MALEINIZED LINSEED OIL PREPARATION

The reactions were performed under a nitrogen atmosphere in a three-neck round-bottom flask, with a molar ratio of linseed oil to maleic anhydride (MA) of 1:1.65 (Lanero et al. 2022). A condenser maintained at 60 °C was connected to the central neck of the flask. The reaction mixture was heated to 200 °C and maintained for 5 h. After completion of the reaction, the mixture was centrifuged at 10,000 rpm for 10 min to separate the unreacted MA (Candy, Vaca-Garcia & Borredon 2005; Lanero et al. 2022).

PREPARATION OF PLA/TPS FILMS FROM PINEAPPLE STEM STARCH

PLA/TPS compounds were prepared by melt blending PLA, TPS, and MLO. The compounding process was carried out using a co-rotating twin-screw extruder (LABTECH Model LTE16-40). The temperature profile during extrusion was set at 100, 120, 140, 150, 160, and 170 °C from the feed zone to the metering zone. The screw speed was maintained at 100 rpm throughout the process. After extrusion, the material was cooled by air and subsequently cut into pellets.

PLA/TPS films were prepared using a blow film machine equipped with a single-screw extruder (LABTECH Model LE20-380/C & LF-250) with a screw diameter of 20 mm and an L/D ratio of 30. The temperature settings from the barrel to the film-blowing die were maintained at 150, 160, 170, and 170 °C, and the screw speed was set at

100 rpm. Films approximately 80 μm thick with a 170 mm width were produced. The different proportions of TPS, PLA, and compatibilizer were summarized in Table 1.

SCANNING ELECTRON MICROSCOPY (SEM)

Scanning electron microscopy (SEM) (Leo Model 1455VP) was employed to characterize the surface morphology and fracture surfaces of the PLA/TPS films after tensile testing. Small pieces of the films were cut and mounted on aluminum stubs using double-sided carbon tape. The samples were then coated with a thin layer of gold and subsequently observed at various magnifications.

TENSILE TEST

Tensile properties of the PLA/TPS films were measured using a universal testing machine (Instron Model 5965). The ASTM D-638 standard procedure was followed in tension mode. The specimens were prepared in a dumbbell shape, with ten specimens tested per sample. The samples were tested in both the machine direction (MD) and the transverse direction (TD). The testing conditions included a gauge length of 57 mm, a crosshead speed of 5 mm/min, and a load cell of 1 N.

DIFFERENTIAL SCANNING CALORIMETER (DSC)

Differential scanning calorimetry (DSC) (Mettler-Toledo Model DSC 5+) was used to investigate the thermal properties of the PLA/TPS films, including the glass transition temperature (T_g), crystallization temperature (T_c), melting temperature (T_m), and degree of crystallinity ($\%X_c$). The samples were first heated from 30 to 200 °C at 10 °C/min, then held at 200 °C for 2 min. They were then cooled to 30 °C at 20 °C/min under a nitrogen (N_2) atmosphere and held for 2 min to eliminate thermal history. A second heating scan was subsequently performed from 30 to 200 °C at 10 °C/min. The crystallinity percentage was calculated using Equation (1).

$$\%\text{Crystallinity } (\%X_c) = \left(\frac{\Delta H_m - \Delta H_{cc}}{\Delta H_{m0} \times \omega_f}\right) \times 100 \quad (1)$$

where ΔH_{m0} is the melting enthalpy of 100% crystalline PLA (93.7 J/g); ΔH_m is the melting enthalpy of the sample; ΔH_{cc} is the cold crystallization enthalpy of the sample; and ω_f is the weight fraction of PLA (Battegazzore, Bocchini & Frache 2011).

DYNAMIC MECHANICAL ANALYZER (DMA)

Dynamic mechanical analysis (DMA) was performed using a TA Instruments Discovery DMA 850. Specimens with dimensions of 26 × 10 × 1 mm³ were prepared and tested in single-cantilever bending mode at 1 Hz and 15 μm amplitude. The temperature range was set from 20 to 120 °C, with a heating rate of 3 °C/min.

FOURIER TRANSFORM INFRARED SPECTROMETER (FT-IR)

The functional groups present in the PLA/TPS films were analyzed using an attenuated total reflectance Fourier transform infrared spectrometer (ATR-FTIR). The spectra were recorded over a wavenumber range of 4000-400 cm^{-1} at a resolution of 4 cm^{-1}, with four scans performed for each sample. The interaction index was subsequently calculated using Equation (2).

$$\text{Interaction index} = \frac{A_{C=O}}{A_{C-H}} \quad (2)$$

where $A_{C=O}$ is the peak area of the C=O stretching and A_{C-H} is the peak area of the C-H stretching.

SOIL DEGRADATION TEST

The biodegradability of the films was evaluated through soil degradation testing. Specimens measuring 50 × 50 mm² were cut into five pieces each, and their initial masses (M_i) were recorded. The specimens were buried to a depth of 4 cm in a controlled soil box. The humidity (50-70% RH) and temperature (approximately 25-30 °C) were maintained, and the moisture content was adjusted to 40-60% by adding water to the soil's water-holding capacity. The samples were removed and weighed every month. After each interval, the samples were retrieved,

TABLE 1. Symbols and proportion of TPS, PLA, and MLO

Samples	PLA (wt%)	TPS (wt%)	MLO (wt%)
PLA	100	-	-
PLA/20TPS	80	20	-
PLA/15TPS/5MLO	80	15	5
PLA/10TPS/10MLO	80	10	10
PLA/20TPS/10MLO	70	20	10
PLA/30TPS/10MLO	60	30	10

washed with water, dried in an oven at 70 °C overnight, and weighed to obtain the final masses (M_f). The percentage of weight loss was calculated using Equation (3).

$$\text{Percentage of weight loss} = \left(\frac{M_i - M_f}{M_i}\right) \times 100 \quad (3)$$

MARINE DEGRADATION TEST

Simulated seawater was prepared according to ASTM D1141-98, and the marine degradation test was conducted in accordance with ASTM D6691-17. Specimens measuring 50 × 50 mm² were cut into five pieces each, and their initial masses (M_i) were recorded. Each specimen was immersed in 100 mL of simulated seawater in sealed containers and incubated at 30 ± 2 °C. The samples were removed and weighed monthly. After each interval, the samples were retrieved, rinsed with water, and dried in an oven at 70 °C overnight, then weighed to determine the final masses (M_f). The percentage of weight loss was calculated in the same way as the soil degradation test.

RESULTS AND DISCUSSION

MORPHOLOGY OF PLA/TPS FILMS AT THE FILM SURFACE

The morphology of the PLA/TPS film surface was investigated by FESEM at 200x magnification (Figure 1). In Figure 1(a), neat PLA exhibited a smooth, homogeneous surface, consistent with its brittle, dense polymeric structure. After the addition of 20 wt% TPS (PLA/20TPS), as Figure 1(b), the surface became significantly rougher, with large, dispersed TPS domains and visible voids, indicating poor interfacial adhesion and phase separation between PLA and TPS due to their incompatibility. In the PLA/15TPS/5MLO blend (Figure 1(c)), the morphology appeared smoother, with fewer and smaller TPS agglomerates, suggesting that MLO partially compatibilized the PLA-TPS interface.

Further addition of MLO and as the TPS content increases in the blends, as shown in Figure 1(d)-1(f). PLA/10TPS/10MLO (Figure 1(d)) showed more homogenous dispersion of TPS, fewer voids, and a smoother surface compared to PLA/20TPS, confirming an improvement of interfacial adhesion and plasticization by MLO (Ferri et al. 2016). PLA/20TPS/10MLO (Figure 1(e)), the number and size of dispersed TPS domains also increase. However, the presence of MLO results in finer dispersion than in blends without MLO, though some phase separation is still visible. However, at high TPS loading in PLA/30TPS/10MLO (Figure 1(f)), the surface became increasingly irregular with numerous TPS-rich domains and interfacial gaps. This suggests that excessive starch disrupted the matrix's continuity, overwhelming the MLO's compatibilization effect. Overall, SEM analysis confirmed that MLO enhances interfacial compatibility between PLA and TPS, though its impact is limited at high TPS contents. The physical characteristics of PLA/TPS films significantly affect their mechanical properties.

MECHANICAL PROPERTIES OF PLA/TPS FILMS

The mechanical properties of the blend films were measured using a Universal Testing Machine, including tensile strength, elongation at break, and Young's modulus, with MLO as a compatibilizer and varying amounts of TPS in the blends. The results are presented in Figure 2. The data indicate a similar trend in TD and MD.

In Figure 2(a) and 2(c), PLA is brittle with a low elongation at break of below 3%, and a tensile strength of 52.31 MPa in the MD direction. The addition of TPS

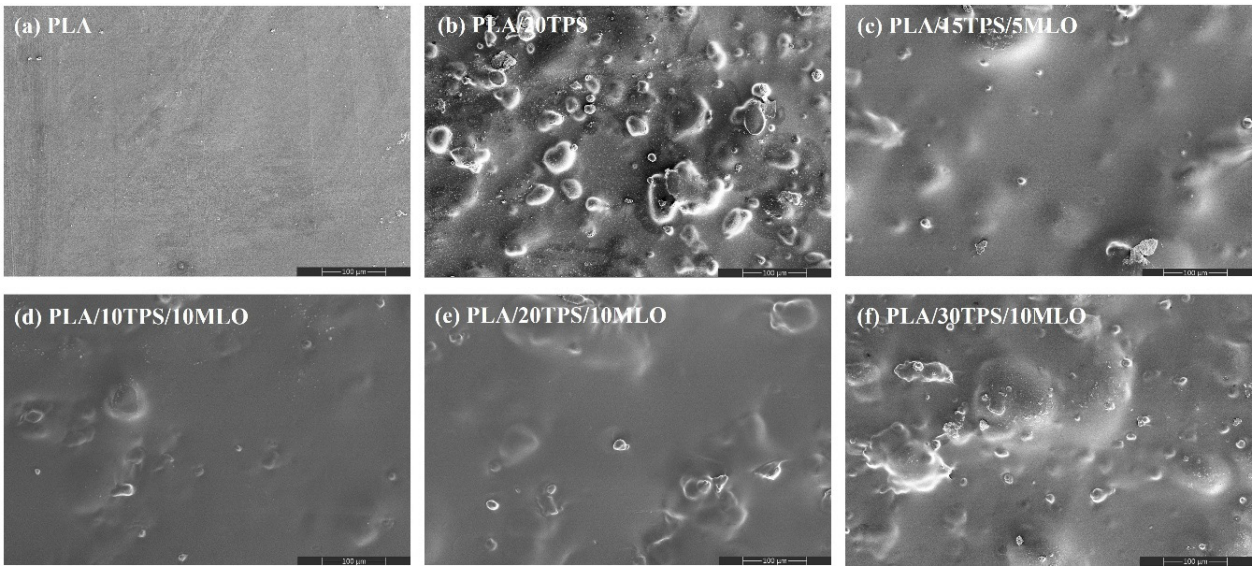

FIGURE 1. FESEM micrographs of the PLA/TPS film surface at 200x magnification of (a-c) with and without MLO, and (d-f) TPS contents

indicates that the lack of miscibility between PLA and TPS reduced blend performance. This is caused by the phase separation of the PLA and TPS phases from the high interfacial tension between the hydrophilic of TPS and the hydrophobic of PLA (Ferri et al. 2017; Jullanun & Yoksan 2020; Ning, Jiugao & Xiaofei 2008; Toh, Lai & Aizan 2011), resulting in a decrease in tensile strength to 32.27 MPa. At the same time, the %elongation at break remains unchanged compared with PLA. MLO improves mechanical ductility by increasing elongation at break to 30.68%, but decreases tensile strength and modulus, indicating a plasticizing effect (Beltrán et al. 2026). MLO can react with the hydroxyl group of PLA, may promote chain extension. On the other hand, MLO can also react with the hydroxyl groups in TPS, resulting in compatibilization between the TPS and PLA phases of MLO, as confirmed by SEM (Ferri et al. 2017, 2016; Hongsriphan et al. 2020). On the other hand, for PLA/15TPS/5MLO, the relatively low MLO content cannot fully compatibilize the polar TPS with the more hydrophobic PLA matrix. As a result, tensile strength decreases due to stress concentration at weak PLA–TPS interfaces. As shown in Figure 2(b) and 2(d), increasing the TPS and MLO content influences the mechanical behavior of the blends. The PLA/10TPS/10MLO formulation appears to be optimal for both compatibilization and plasticization. At this ratio, MLO is present in sufficient quantity to achieve a maximum elongation at break of 43.21%, indicating a more ductile and tough material (Fonseca-García et al. 2022).

Increasing TPS content to 20 wt% and 30 wt% TPS results in tensile strength and elongation at break decreasing to 30.53% and 21.51%, respectively, compared to PLA/10TPS/10MLO. That reflects poorer stress transfer and reduced matrix continuity. Elongation at break is also diminished, indicating brittle-like failure due to stress concentration at unbonded TPS-rich domains. The morphology is likely characterized by large TPS aggregates and weak interfaces, leading to premature crack initiation and propagation under tensile stress.

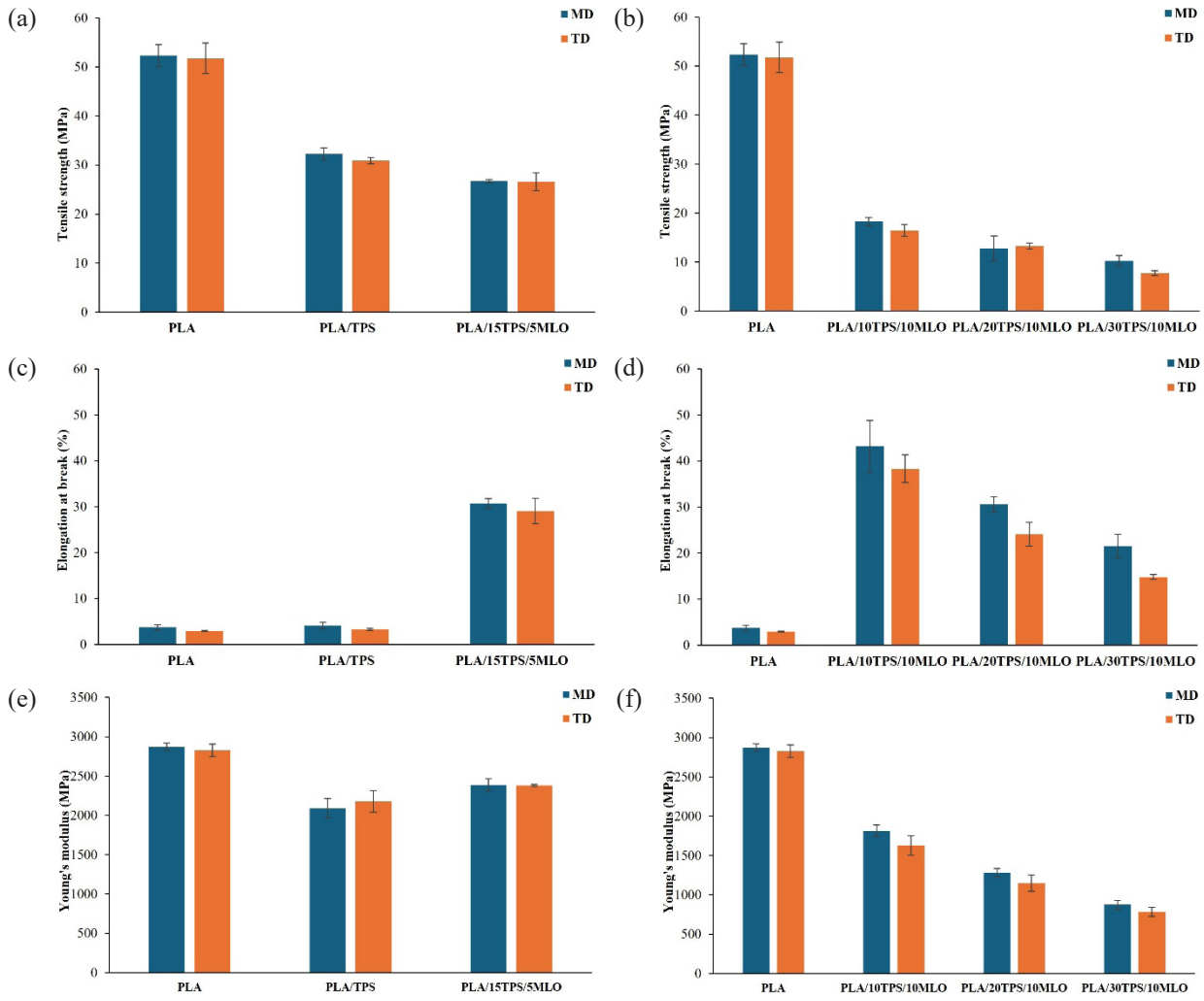

FIGURE 2. Tensile properties of the PLA/TPS films with, without MLO content and the TPS contents vary

MORPHOLOGY OF PLA/TPS FILMS AT THE SURFACE FRACTURE

The morphology of the PLA/TPS films surface fracture of the PLA/TPS films from the tensile test at 1000x magnification is shown in Figure 3. The effect of MLO as a compatibilizer and the impact of the TPS content proportion in the blends are also shown. In Figure 3, PLA exhibits brittle behavior, with a smooth, flat fracture surface, characteristic of a brittle semi-crystalline polymer. The addition of 20% wt TPS (PLA/20TPS) (Figure 3(b)) exhibits clear signs of phase separation, such as starch granule pull-outs and voids. This indicates a lack of interaction between the PLA and TPS phases, which is attributed to the low adhesion of hydrophilic TPS to hydrophobic PLA. However, the introduction of MLO improved the morphological characteristics of the blends. PLA/15TPS/5MLO (Figure 3(c)) shows that morphology likely consists of discrete TPS domains within a PLA-rich matrix. The surface appeared more ductile, with visible fibrils and reduced voids, suggesting that MLO enhanced compatibility by promoting stronger interfacial bonding between the polymer phases. This is evident in the increase in % elongation for PLA/15TPS/5MLO, as shown in Figure 2(c). This semi-compatibilized state improves toughness compared to PLA/20TPS binary blends (Trinh, Tadele & Mekonnen 2022).

Increasing TPS concentrations to 10, 20, and 30 wt% with 10 wt% MLO (Figure 3(d)-3(f)) shows that phase separation increases. It becomes highly irregular and rough, with large, distinct TPS domains growing through agglomeration, resulting in more homogeneously dispersed TPS domains and fewer gaps at the interfaces. The increased TPS content overwhelms the compatibilizing effect of MLO, large TPS aggregates, and weak interfaces, leading to premature crack initiation and propagation (Liminana et al. 2019). The results show a decrease in the PLA/TPS film's percentage elongation, as shown in Figure 2(a).

DYNAMIC MECHANICAL THERMAL PROPERTIES OF PLA/TPS FILMS

The dynamic mechanical thermal properties of PLA/TPS films were measured using a Dynamic Mechanical Analyzer (DMA), including the storage modulus and tan (δ), with the effects of MLO as a compatibilizer (a), and the amounts of TPS in the blends (b). The results are presented in Figure 4. Figure 4(a) shows the DMA results of storage modulus (E′) as a function of temperature. At room temperature, PLA exhibited the highest storage modulus (E′) values above 100 MPa, reflecting its rigid, semi-crystalline nature. The addition of TPS and MLO resulted in a substantial reduction in E′ across the entire temperature range. PLA/20TPS: TPS reduces the material's stiffness due to the immiscibility of the rich-phase PLA with the polymeric TPS chain, as evidenced by phase separation. However, when 5% MLO is added (PLA/15TPS/5MLO), the modulus improves relative to PLA/20TPS, especially in the rubbery region (>70 °C). This suggests that MLO enhances compatibility between PLA and TPS, resulting in improved mechanical integrity and enhanced load transfer across phases. The smoother transition at the T_g 60 °C in the MLO-containing blend also indicates better phase dispersion and reduced brittleness. Further inclusion of MLO in PLA/15TPS/5MLO led to an even more significant compatibilization of MLO and a

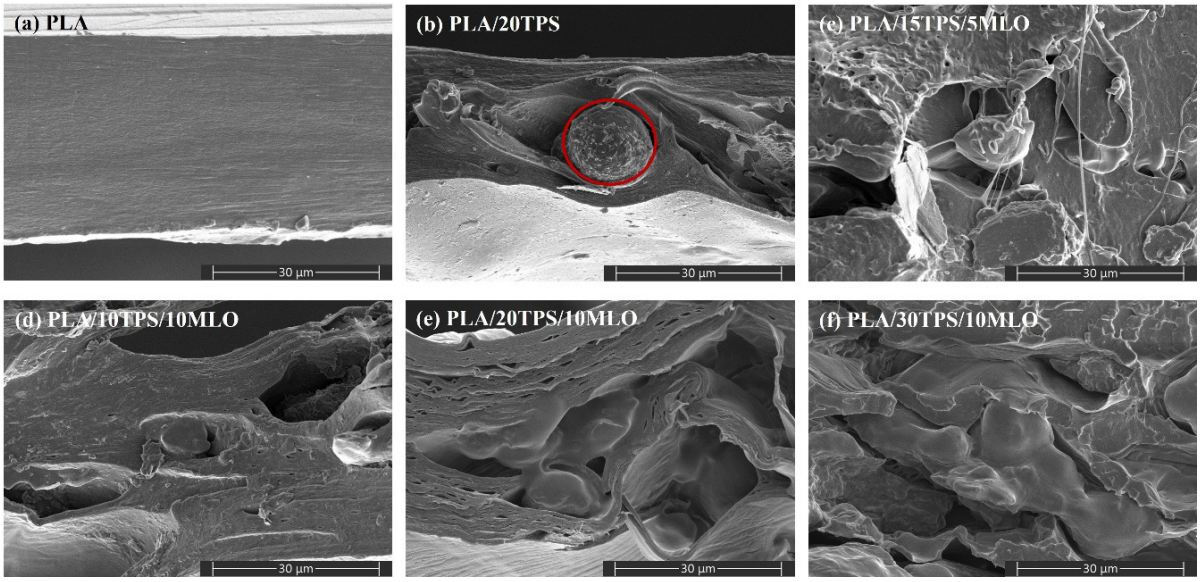

FIGURE 3. FESEM micrographs of the fracture surface from the tensile test at 1000 magnification, (a-c) with and without MLO, and (d-f) TPS contents

shift of the T_g, slightly shifted tan (δ) peak (Figure 4(a)), suggesting enhanced interfacial interaction and increased molecular motion due to the plasticizing effect of MLO. This also implies improving miscibility and reducing phase separation compared to the uncompatibilized PLA/20TPS blend. All those results agree with the thermal properties reported in Table 2.

Figure 4(b) shows that as the TPS content increases, the overall storage modulus decreases, particularly in the glassy and rubbery regions of the material. PLA/10TPS/10MLO shows the highest modulus among the samples, indicating that lower TPS content better preserves PLA stiffness. The downward trend in modulus with increasing TPS content in PLA/20TPS/10MLO and PLA/30TPS/10MLO, which is reflected in the decrease in E′ values, suggests significantly reduced intermolecular interactions. This trend reflects the softening effect of TPS and the limitations of compatibilizer efficiency at higher TPS loadings. These results demonstrate that while MLO significantly improves interfacial adhesion and modulus, excessive TPS content directly affects the mechanical performance of the blends (Ferri et al. 2017, 2016; Lerma-Canto et al. 2021).

THERMAL PROPERTIES OF THE BLEND FILMS

The thermal properties of PLA/TPS films were measured using a Differential Scanning Calorimeter (DSC), including T_g, T_{cc}, and T_m with the effects of MLO as a compatibilizer (a), and the amount of TPS in the blends (b). Figure 5(a) presents PLA, which exhibited a T_g around 54.07 °C, a T_{cc} near 110 °C, and a T_m at approximately 150 °C, which are characteristic of semi-crystalline PLA with 1.88% of crystallinity of PLA. Incorporation of TPS (PLA/20TPS), T_g slightly decreased (52.06 °C), indicating increased chain mobility due to the partial plasticization effect of TPS and the possible phase separation that reduces PLA–PLA interactions. The T_{cc} also decreased, suggesting that TPS may act as a nucleating agent, promoting earlier crystallization during heating. With the addition of MLO (PLA/20TPS), a more pronounced decrease in T_g to 47.59 °C was observed, confirming its dual role as a plasticizer and compatibilizer with MLO. MLO improves the interfacial adhesion between PLA and TPS by reacting with hydroxyl groups, enhancing miscibility and disrupting the crystallinity of the PLA/15TPS/5MLO, reducing it to 4.94% from 6.55% in PLA/20TPS. The T_m remained relatively stable across all samples, indicating that the crystalline regions of PLA are preserved despite morphological changes. These thermal transitions reflect the complex interplay between plasticization, phase compatibility, and crystallization kinetics within the ternary PLA/TPS/MLO system.

In Figure 5(b), while increasing MLO content to 10% (PLA/10TPS/10MLO), the crystallinity decreases to 0.41%, attributing to a more compatible blend compared with PLA/15TPS/5MLO. However, at higher TPS contents, MLO shows crystallinity of 2.15% in PLA/20TPS/10MLO

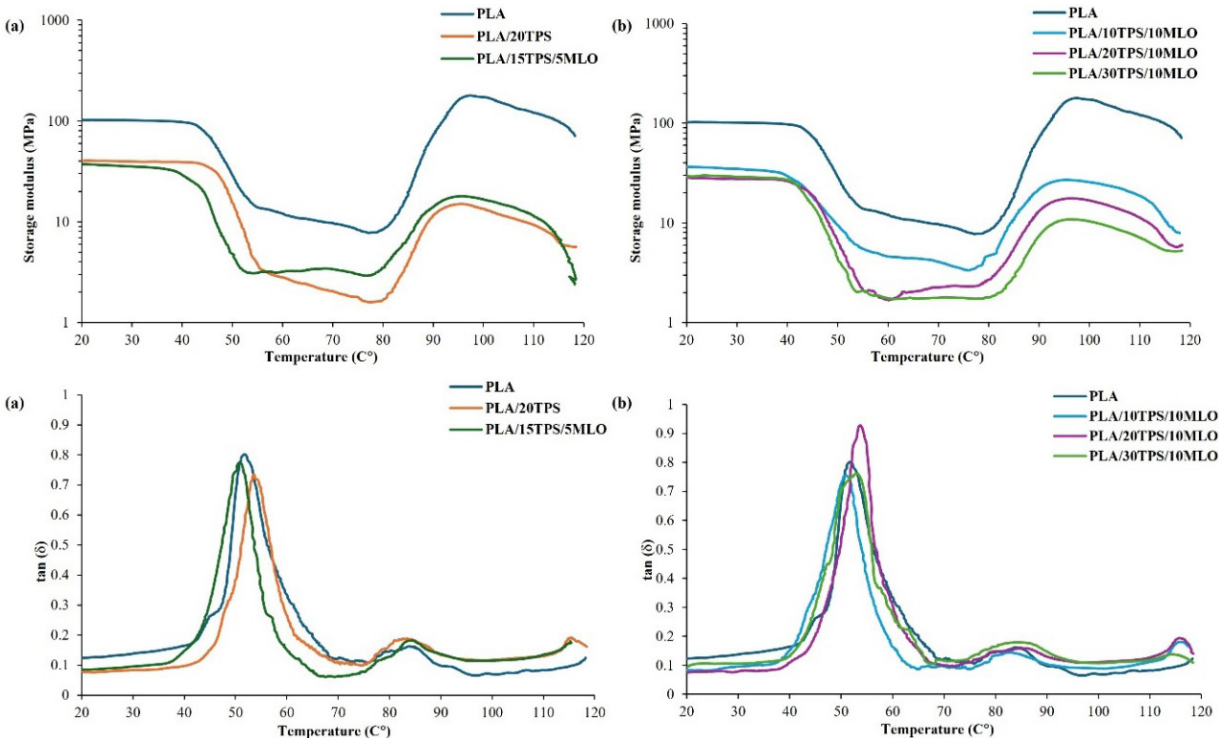

FIGURE 4. Storage modulus and tan (δ) of the PLA/TPS films (a) with and without MLO, and (b) TPS contents

and 4.65% in PLA/30TPS/10MLO, indicating a decrease in crystallinity. This is due to the formation of phase-separated TPS-rich domains and excessive disruption of PLA chain packing, which interferes with crystal growth. T_g decreases gradually 50.28 °C for PLA/20TPS/10MLO, and 49.75 °C for PLA/30TPS/10MLO. This shift reflects enhanced chain mobility, primarily due to reduced segmental cohesion in PLA chains resulting from interfacial incompatibility with TPS. However, the T_{cc} decreased to 114.69 °C and 111.10 °C in PLA/20TPS/10MLO and PLA/30TPS/10MLO, respectively. This indicates that even TPS may act as a nucleating agent, the compatibilizing effect of MLO at higher TPS loading slows down crystallization. This improves miscibility, which restricts chain reorganization (Ferri et al. 2017, 2016; Liminana et al. 2019; Przybytek et al. 2018; Trinh, Tadele & Mekonnen 2022; Wang et al. 2008).

FUNCTIONAL GROUP OF THE BLEND FILMS

Figure 6 and Table 3 illustrate the impact of MLO on the chemical environment and phase adhesion of PLA/TPS blends. The FTIR spectra shows characteristic bands for all samples: the carbonyl (C=O) stretching at 1746 cm^{-1}, $-CH_3$ bending at 1453 cm^{-1}, C-O stretching within the ester groups at 1179 cm^{-1}, and C-O-C stretching at 865 cm^{-1}. The addition of MLO as a compatibilizer resulted in a notable increase in the interaction index, from 5.03 for PLA/20TPS to 5.28 for PLA/15TPS/5MLO. This upward shift indicates a higher density of chemical interactions and suggests that the MLO effectively bridges the immiscible phases (Chieng et al. 2014). Although the clear disappearance of anhydride peaks could not be conclusively resolved due to overlap in the blend spectra, additional FTIR analysis using an interaction index together with mechanistic interpretation, has been included as indirect evidence supporting compatibilization.

Specifically, the increased index confirms that the maleic anhydride groups in the MLO have undergone ring-opening reactions with the hydroxyl (-OH) groups of the starch and the PLA chain. This reactive compatibilization transforms the weak physical interface into a more cohesive network of covalent ester bonds. These findings align with the observations confirming that while native PLA/TPS blends exhibit minimal compatibility, the inclusion of MLO significantly enhances interfacial adhesion through these targeted chemical interactions (Ferri et al. 2016; Khairuddin et al. 2016). Figure 7 shows the proposed mechanism of interaction between PLA/TPS and MLO as a compatibilizer.

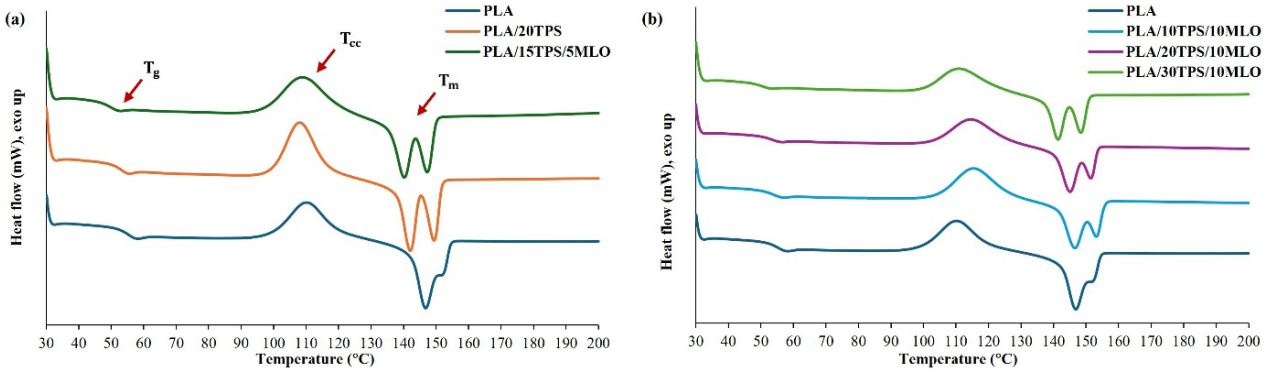

FIGURE 5. DSC heating thermograms of the PLA/TPS films (a) with and without MLO, and (b) TPS content

TABLE 2. Thermal properties of PLA/TPS films

Samples	T_g (°C)	T_{cc} (°C)	T_{m1} (°C)	T_{m2} (°C)	ΔH_f (J/g)	$\%X_c$
PLA	54.07	110.20	146.73	151.42	27.19	1.88
PLA/20TPS	52.06	108.14	141.99	149.34	31.86	6.55
PLA/15TPS/5MLO	47.59	109.03	140.07	147.25	31.48	4.94
PLA/10TPS/10MLO	50.25	115.44	146.47	153.16	25.77	0.41
PLA/20TPS/10MLO	50.28	114.69	144.95	151.47	22.53	2.15
PLA/30TPS/10MLO	49.75	111.10	141.28	148.37	22.66	4.65

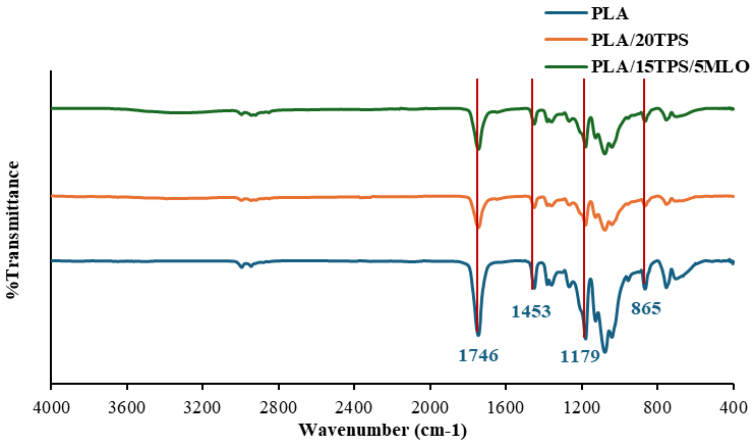

FIGURE 6. FTIR spectra of PLA and PLA/TPS with and without MLO

TABLE 3. Interaction index of the blend films

Samples	Interaction index
PLA/20TPS	5.03
PLA/15TPS/5MLO	5.28

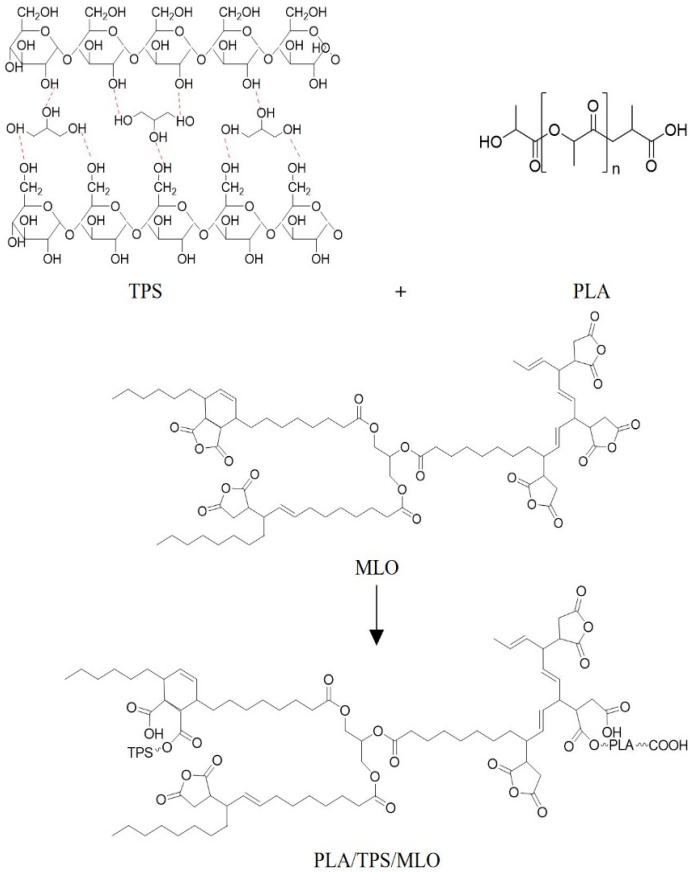

FIGURE 7. The reaction of PLA/TPS/MLO (Clasen, Müller & Pires 2015; Ferri et al. 2017)

SOIL DEGRADATION

Figure 8(a) shows that PLA exhibits minimal degradation over 3 months, as it degrades slowly in soil due to its semi-crystalline structure and poor water uptake. PLA has been shown to possess inherent hydrophobicity and a crystalline structure that limits microbial growth and attack. Remains essentially unchanged in appearance, supporting the observation of minimal weight loss. PLA/20TPS exhibits a significant increase, reaching approximately 11% within 3 months. TPS is hydrophilic and sensitive to microbial and hydrolytic degradation, acting as a catalyst for degradation. As TPS breaks down (Adam, Osman & Shamsudin 2018), it creates porosity and pathways for moisture entrance, indirectly accelerating PLA degradation in PLA/20TPS. Weight loss increases steadily over time, reaching the highest value across all samples after 3 months. Visible signs of surface erosion and discoloration indicate active degradation as seen in Figure 8(a). Adding MLO (PLA/15TPS/5MLO) decreased degradation. It shows intermediate weight loss (around 7%), higher than pure PLA but generally lower than PLA/20TPS. MLO may act as a barrier to water diffusion due to its hydrophobic chains. It may improve interfacial adhesion, reduce voids, and decrease the accessibility of TPS domains to microorganisms. This can be observed from surface changes, which are less pronounced than in PLA/20TPS, consistent with the intermediate weight-loss data (Song et al. 2009).

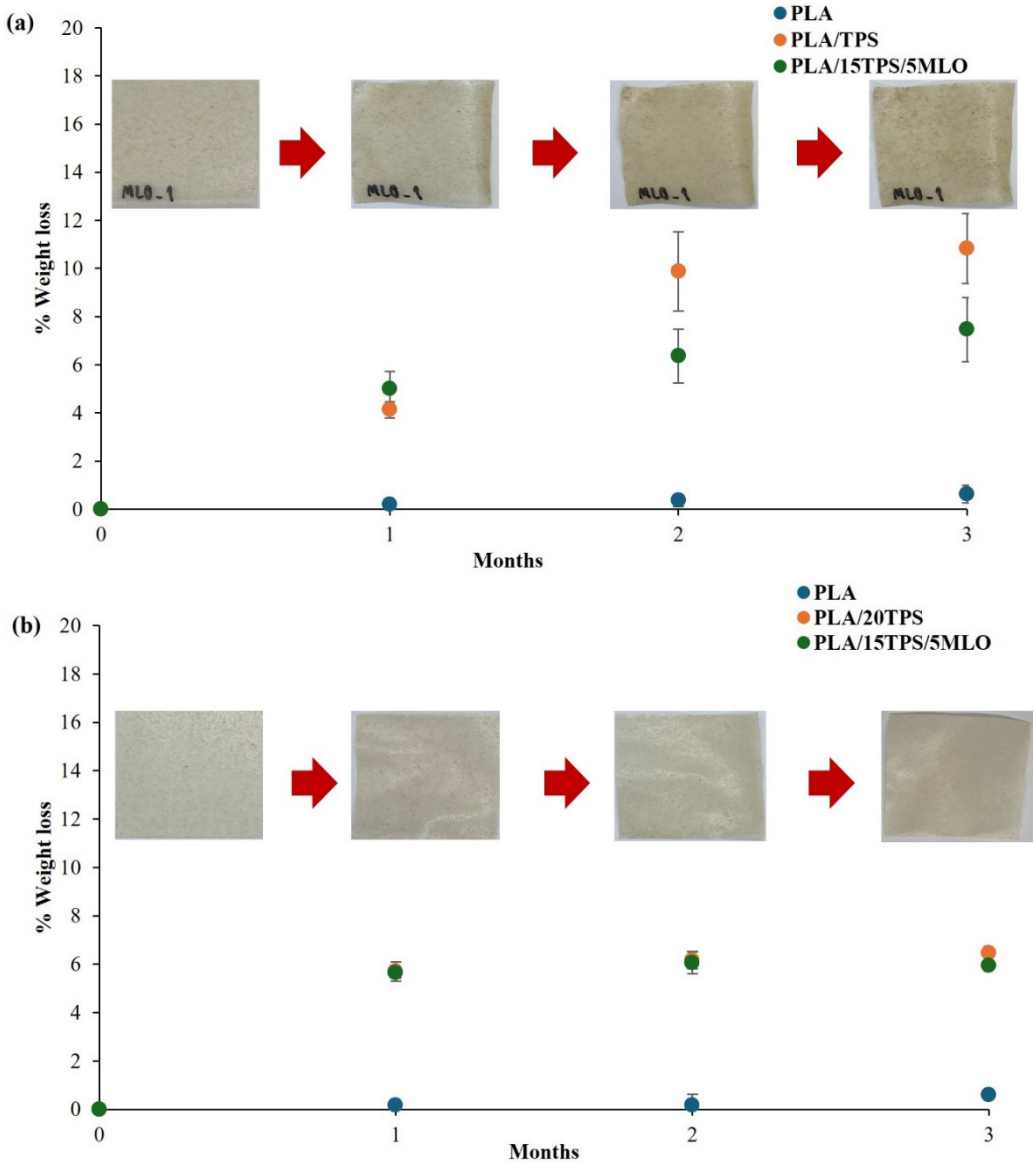

FIGURE 8. %weight loss of the films from the (a) soil degradation test and (b) marine degradation test

MARINE DEGRADATION

PLA, negligible degradation around 1% or less, consistent with the known resistance of PLA in aquatic environments. This hinders water uptake and microbial attacks. The visual appearance remains relatively unchanged, consistent with minimal weight loss and low degradation. Both PLA/TPS with and without MLO exhibit similar trends, characterized by rapid early-stage degradation, reaching approximately 6-7% in 1 month. TPS dissolves or swells in water, promoting early mass loss. Figure 8(b) shows the surface film changes, which become cloudy, rough, and discolored, indicating active degradation and erosion, consistent with the high weight loss data. MLO (PLA/15TPS/5MLO) does not significantly change the marine degradation rate after the initial month. Because MLO acts as a compatibilizer, improving the blend's homogeneity, which can slightly slow down the degradation compared to PLA/20TPS, but the material remains much more biodegradable than neat PLA, possibly because marine microbes are less capable of breaking down MLO-modified surfaces. MLO limits water uptake after the initial rush of TPS degradation (Ferri et al. 2016; Hamzah et al. 2011; Song et al. 2009; Thirmizir & Mohd Ishak 2013).

While the inclusion of TPS accelerates biodegradation, the slight reduction in degradation rate observed in MLO-containing blend films represents a significant functional advantage for flexible packaging applications. Pure TPS films are notoriously susceptible to moisture ingress, which leads to rapid loss of structural integrity and dimensional instability under humid conditions. The hydrophobic fatty acid chains of MLO act as a barrier to water diffusion, effectively mitigating this weakness. This dual functionality, providing environmental degradability while maintaining storage stability, positions the developed bioplastic as a viable industrial alternative to non-degradable polyolefins. In terms of mechanical strength, the experimental film exhibited a tensile strength of 18.26 MPa, within the typical range reported for LDPE films (8-25 MPa) (ASTM 2015; Laird Plastics 2026; TP Plastic USA 2026). This strength suggests that thin PLA/TPS films can be utilized to achieve the same load-bearing capacity as thicker LDPE films, reducing total material consumption (Krupińska & Korzeniowska 2025).

However, a functional gap in ductility remains: while reactive compatibilization with MLO increased elongation at break to 43.21%, it is still an order of magnitude lower than LDPE's exceptional stretchability (400-800%). This indicates that while the developed bioplastic may not yet replace LDPE in high-stretch applications like pallet wrap, it is highly suitable for 'semi-rigid' flexible formats such as stand-up pouches, lidding films, or stable liners where structural stiffness (Modulus 1814.63 MPa vs. LDPE's 150-250 MPa) is prioritized.

CONCLUSIONS

This work demonstrates a sustainable strategy for producing biodegradable PLA-based films by integrating TPS derived from pineapple stem waste and MLO as a fully bio-based compatibilizer. The incorporation of TPS contributed to partial biodegradability and reduced material cost. While MLO significantly enhanced interfacial adhesion between PLA and TPS phases, improving elongation at break and overall ductility. Among all formulations, PLA/10TPS/10MLO exhibited the most balanced combination of tensile strength, ductility, morphology, and biodegradability and was identified as the optimal composition. From blown film processing with a 170 mm width and 80 microns thick. An increase of about 14 times in elongation compared with PLA. Thermal analysis confirmed increased chain mobility, and FESEM showed more homogeneous morphologies with fewer voids in the MLO-containing blends. Soil burial and marine degradation tests further indicated enhanced degradation rates in PLA/TPS/MLO compared to neat PLA, which increased by 7 times. The dual use of agricultural starch waste and a reactive, plant-derived compatibilizer to tailor the mechanical and degradation properties of PLA without synthetic plasticizers or petroleum-based additives was reported. The films developed herein hold promise for single-use applications and flexible packaging; reduced brittleness and environmental degradability are critical performance characteristics.

ACKNOWLEDGEMENTS

Hataithip Sanpromma thanks the Faculty of Science, Naresuan University, for the financial support of her tuition fees. Taweechai Amornsakchai acknowledges the support provided by Mahidol University (Fundamental Fund: fiscal year 2023 by the National Science Research and Innovation Fund (NSRF); Grant No. FF-069/2566).

REFERENCES

Aboubakar, Njintang, Y.N., Scher, J. & Mbofung, C.M.F. 2008. Physicochemical, thermal properties and microstructure of six varieties of taro (*Colocasia esculenta* L. Schott) flours and starches. *Journal of Food Engineering* 86(2): 294-305. https://doi.org/10.1016/j.jfoodeng.2007.10.006

Adam, S.N.F.S., Osman, A.F. & Shamsudin, R. 2018. Tensile properties, biodegradability and bioactivity of thermoplastic starch (TPS)/bioglass composites for bone tissue engineering. *Sains Malaysiana* 47(6): 1303-1310. http://dx.doi.org/10.17576/jsm-2018-4706-27

Akrami, M., Ghasemi, I., Azizi, H., Karrabi, M. & Seyedabadi, M. 2016. A new approach in compatibilization of the poly(lactic acid)/thermoplastic starch (PLA/TPS) blends. *Carbohydrate Polymers* 144: 254-262. https://doi.org/10.1016/j.carbpol.2016.02.035

ASTM. 2015. *Standard Specification for Polyethylene Film and Sheeting (ASTM D2103- 15)*. West Conshohocken: ASTM International. https://store.astm.org/d2103-15.html

Atiwesh, G., Mikhael, A., Parrish, C.C., Banoub, J. & Le, TAT. 2021. Environmental impact of bioplastic use: A review. *Heliyon* 7(9): e07918. https://doi.org/10.1016/j.heliyon.2021.e07918

Battegazzore, D., Bocchini, S. & Frache, A. 2011. Crystallization kinetics of poly(lactic acid)-talc composites. *eXPRESS Polymer Letters* 5(10): 849-858. https://doi.org10.3144/expresspolymlett.2011.84

Beltrán, F.R., Dominici, F., Agüero, Á., Lascano, D., Arrieta, M.P., Balart, R. & Puglia, D. 2026. Upgrading of mechanically recycled poly (lactic acid) by use of maleinized linseed oil. *Industrial Crops & Products* 244: 123175. https://doi.org/10.1016/j.indcrop.2026.123175

Candy, L., Vaca-Garcia, C. & Borredon, M-E. 2005. Synthesis and characterization of oleic succinic anhydrides: Structure-property relations; Synthesis and characterization of oleic succinic anhydrides: Structure-property relations. *American Oil Chemists' Society* 82(4): 271-277. https://doi.org/10.1007/s11746-005-1066-5

Chieng, B.W., Ibrahim, N.A., Yunus, W.M.Z.W. & Hussein, M.Z. 2014. Poly(lactic acid)/poly(ethylene glycol) polymer nanocomposites: Effects of graphene nanoplatelets. *Polymers* 6(1): 93-104. https://doi.org/10.3390/polym6010093

Chu, P.H., Jenol, M.A., Phang, L.Y., Ibrahim, M.F., Prasongsuk, S, Bankeeree, W., Punnapayak, H., Lotrakul, P. & Abd-Aziz, S. 2021. Starch extracted from pineapple (*Ananas comosus*) plant stem as a source for amino acids production. *Chemical and Biological Technologies in Agriculture* 8(1): 29. https://doi.org/10.1186/s40538-021-00227-6

Clasen, S.H., Müller, C.M.O. & Pires, A.T.N. 2015. Maleic anhydride as a compatibilizer and plasticizer in TPS/PLA blends. *Brazilian Chemical Society* 26(8): 1583-1590. http://dx.doi.org/10.5935/0103-5053.20150126

Ferrarezi, M.M.F., de Oliveira Taipina, M., da Silva, L.C.E. & Gonçalves, M.d.C. 2013. Poly(ethylene glycol) as a compatibilizer for poly(lactic acid)/thermoplastic starch blends. *Polymers and the Environment* 21(1): 151-159. https://doi.org/10.1007/s10924-021-02207-1

Ferri, J.M., Garcia-Garcia, D., Montanes, N., Fenollar, O. & Balart, R. 2017. The effect of maleinized linseed oil as biobased plasticizer in poly(lactic acid)-based formulations. *Polymer International* 66(6): 882-891. https://doi.org/10.1002/pi.5329

Ferri, J.M., Garcia-Garcia, D., Sánchez-Nacher, L., Fenollar, O. & Balart, R. 2016. The effect of maleinized linseed oil (MLO) on mechanical performance of poly(lactic acid)-thermoplastic starch (PLA-TPS) blends. *Carbohydrate Polymers* 147: 60-68. https://doi.org/10.1016/j.carbpol.2016.03.082

Fonseca-García, A., Osorio, B.H., Aguirre-Loredo, R.Y., Calambas, H.L. & Caicedo, C. 2022. Miscibility study of thermoplastic starch/polylactic acid blends: Thermal and superficial properties. *Carbohydrate Polymers* 293: 119744. https://doi.org/10.1016/j.carbpol.2022.119744

Hongsriphan, N., Kamsantia, P., Sillapasangloed, P. & Loychuen, S. 2020. Bio-based composite from poly(butylene succinate) and peanut shell waste adding maleinized linseed oil. *IOP Conf. Series: Materials Science and Engineering* 773: 012046. https://doi.org/10.1088/1757-899X/773/1/012046

TP Plastic. *How Plastic Bag Strength Is Tested: From Load Capacity to Puncture Resistance.* Plastic bags & packaging manufacture TPPlastic USA. https://tpplasticusa.com/20-10-25-plastic-bag-strength/ (Accessed 9 April 2026).

Japheth, K.A. & John, B. 2018. Physicochemical properties of starches extracted from local cassava varieties with the aid of crude pectolytic enzymes from *Saccharomyces cerevisiae* (ATCC 52712). *African Journal of Food Science* 12(7): 151-164. https://doi.org/10.5897/AJFS2018.1701

Jullanun, P. & Yoksan, R. 2020. Morphological characteristics and properties of TPS/PLA/cassava pulp biocomposites. *Polymer Testing* 88: 106522. https://doi.org/10.1016/j.polymertesting.2020.106522

Khairuddin, Pramono, E., Utomo, S.B., Wulandari, V., Zahrotul, A.W. & Clegg, F. 2016. FTIR studies on the effect of concentration of polyethylene glycol on polymerization of Shellac. *Physics: Conference Series* 776: 012053. https://doi.org/10.1088/1742-6596/776/1/012053

Krupińska, K. & Korzeniowska, M. 2025. Comparison of the properties of compostable and conventional LDPE films. *Sustainability* 17(17): 7867. https://doi.org/10.3390/su17177867

Lanero, F., Bresolin, B.M., Scettri, A., Nogarole, M., Schievano, E., Mammi, S., Saielli, G., Famengo, A., Semenzato, A. & Tafuro, G. 2022. Activation of vegetable oils by reaction with maleic anhydride as a renewable source in chemical processes: New experimental and computational NMR evidence. *Molecules* 27(23): 8142. https://doi.org/10.3390/molecules27238142

Li, L., Chin, S.X., Rachtanapun, P., Amornsakchai, T., Khiew, P.S., Chowdhury, S., Zakaria, S. & Chia, C.H. 2025. Cellulose nanocrystals and zinc oxide in pineapple starch films for enhanced banana shelf-life. *Sains Malaysiana* 54(3): 899-911. http://doi.org/10.17576/jsm-2025-5403-21

Lerma-Canto, A., Gomez-Caturla, J., Herrero-Herrero, M., Garcia-Garcia, D. & Fombuena, V. 2021. Development of polylactic acid thermoplastic starch formulations using maleinized hemp oil as biobased plasticizer. *Polymers* 13(9): 1392. https://doi.org/10.3390/polym13091392

Liminana, P., Garcia-Sanoguera, D., Quiles-Carrillo, L., Balart, R. & Montanes, N. 2019. Optimization of maleinized linseed oil loading as a biobased compatibilizer in poly(butylene succinate) composites with almond shell flour. *Materials* 12(5): 685. https://doi.org/10.3390/ma12050685

Logam, P., Bagi, B., Masin, I.A., Ditangkap, Y., Perairan, D. & Dickson, P. 2015. Assessment of heavy metal in self-caught saltwater fish from Port Dickson coastal water, Malaysia. *Sains Malaysiana* 44(1): 91-99. https://doi.org/10.17576/jsm-2015-4401-13

Laird Plastics. *Low-Density Polyethylene (LDPE): Complete Technical Guide*. https://lairdplastics.com/resources/lowdensity-polyethylene-ldpe- complete-technicalguide/?srsltid=AfmBOopnSSDRLGADso7Oga5WBwMIvYFXy8OZOL4QJsE1VmIHOHBaYVlO (Accessed 9 April 2026).

Mallick, N., Pattanayak, D.S., Soni, A.B. & Pal, D. 2020. Starch based polymeric composite for food packaging applications. *Engineering Research and Application* 10(4): 11-34. https://doi.org/10.9790/9622-1004021134

Hamzah, A., Kipli, S.H., Una, R., Ismail, S.R. & Sarmani, S. 2011. Microbiological study in coastal water of Port Dickson, Malaysia. *Sains Malaysiana* 40(2): 93-99. https://www.ukm.my/jsm/pdf_files/SM-PDF-40-2-2011/03%20Ainon.pdf

Nakthong, N., Wongsagonsup, R. & Amornsakchai, T. 2017. Characteristics and potential utilizations of starch from pineapple stem waste. *Industrial Crops and Products* 105: 74-82. https://doi.org/10.1016/j.indcrop.2017.04.048

Nihart, A.J., Garcia, M.A., El Hayek, E., Liu, R., Olewine, M., Kingston, J.D., Castillo, E.F., Gullapalli, R.R., Howard, T. & Bleske, B. 2025. Bioaccumulation of microplastics in decedent human brains. *Nature Medicine* 31(4): 1114-1119. https://doi.org/10.1038/s41591-024-03453-1

Ning, W., Jiugao, Y. & Xiaofei, M. 2008. Preparation and characterization of compatible thermoplastic dry starch/poly(lactic acid). *Polymer Composites* 29(5): 551-559. https://doi.org/10.1002/pc.20399

Park, J.W., Im, S.S., Kim, S.H. & Kim, Y.H. 2000. Biodegradable polymer blends of poly(L-lactic acid) and gelatinized starch. *Polymer Engineering & Science* 40(12): 2539-2550. https://doi.org/10.1002/pen.11384

Przybytek, A., Sienkiewicz, M., Kucińska-Lipka, J. & Janik, H. 2018. Preparation and characterization of biodegradable and compostable PLA/TPS/ESO compositions. *Industrial Crops and Products* 122: 375-383. https://doi.org/10.1016/j.indcrop.2018.06.016

Sarazin, P., Li, G., Orts, W.J. & Favis, B.D. 2008. Binary and ternary blends of polylactide, polycaprolactone and thermoplastic starch. *Polymer* 49(2): 599-609. https://doi.org/10.1016/j.polymer.2007.11.029

Seung, D. 2020. Amylose in starch: Towards an understanding of biosynthesis, structure and function. *New Phytologist* 228(5): 1490-1504. https://doi.org/10.1111/nph.16858

Shlosman, K., Suckeveriene, R.Y., Rosen-Kligvasser, J., Tchoudakov, R., Zelikman, E., Semiat, R. & Narkis, M. 2014. Controlled migration of antifog additives from LLDPE compatibilized with LLDPE grafted maleic anhydride. *Polymers for Advanced Technologies* 25(12): 1484-1491. https://doi.org/10.1002/pat.3390

Song, J.H., Murphy, R.J., Narayan, R. & Davies, G.B.H. 2009. Biodegradable and compostable alternatives to conventional plastics. *Philosophical Transactions B* 364(1526): 2127-2139. https://doi.org/10.1098/rstb.2008.0289

Thirmizir, M.Z.A. & Mohd Ishak, Z.A. 2013. Effect of maleated compatibiliser (PBS-g-MA) addition on the flexural properties and water absorption of poly(butylene succinate)/kenaf bast fibre composites. *Sains Malaysiana* 42(4): 435-441. https://www.ukm.my/jsm/pdf_files/SM-PDF-42-4-2013/02%20M.Z.%20Ahmad%20Thirmizir.pdf

Toh, W.Y., Lai, J.C. & Aizan, W.A.R.W. 2011. Influence of compounding methods on poly(vinyl) alcohol/sago pith waste biocomposites. *Composite Materials* 45(11): 1201-1207. http://journalarticle.ukm.my/2546/1/08_W.Y._Toh.pdf

Trinh, B.M., Tadele, D.T. & Mekonnen, T.H. 2022. Robust and high barrier thermoplastic starch - PLA blend films using starch-graft-poly(lactic acid) as a compatibilizer. *Materials Advance* 3(15): 6208-6221. https://doi.org/10.1039/d2ma00501h

Wang, N., Yu, J., Chang, P.R. & Ma, X. 2008. Influence of formamide and water on the properties of thermoplastic starch/poly(lactic acid) blends. *Carbohydrate Polymers* 71(1): 109-118. https://doi.org/10.1016/j.carbpol.2007.05.025

*Corresponding author; email: supatraw@nu.ac.th